Kai Xu[1]
RII Lab (Laboratory of Robotics Innovation and Intervention),
UM-SJTU Joint Institute,
Shanghai Jiao Tong University,
800 Dongchuan Road,
Shanghai 200240, China
e-mail: k.xu@sjtu.edu.cn

Jiangran Zhao
RII Lab (Laboratory of Robotics Innovation and Intervention),
UM-SJTU Joint Institute,
Shanghai Jiao Tong University,
800 Dongchuan Road,
Shanghai 200240, China
e-mail: zjr318@sjtu.edu.cn

Dong Qiu
RII Lab (Laboratory of Robotics Innovation and Intervention),
UM-SJTU Joint Institute,
Shanghai Jiao Tong University,
800 Dongchuan Road,
Shanghai 200240, China
e-mail: d.qiu@sjtu.edu.cn

You Wang
RII Lab (Laboratory of Robotics Innovation and Intervention),
UM-SJTU Joint Institute,
Shanghai Jiao Tong University,
800 Dongchuan Road,
Shanghai 200240, China
e-mail: youwang@sjtu.edu.cn

A Pilot Study of a Continuum Shoulder Exoskeleton for Anatomy Adaptive Assistances

Many existing exoskeletons have followed a similar design concept that a rigid kinematic chain is actuated to mobilize a human wearer in spite of the intended applications. For performance-augmenting applications where an exoskeleton is usually paired with a specific wearer, the human–machine kinematic compatibility might be well maintained. However, in a clinical setting for rehabilitation where one exoskeleton is often shared by a group of patients, it will be difficult for the therapists to guarantee the on-site adjustments would accurately fit the exoskeleton to each individual patient with his/her unique anatomy. This paper proposes a continuum shoulder exoskeleton design to realize anatomy adaptive assistances (AAAs) for hemiparetic patients in a purely assistive mode where patient's limb motions are passive. The shoulder exoskeleton conforms to distinct human anatomies adaptively due to its intrinsic flexibility but still manages to deliver motion assistances in a consistent way. The design concept and the system descriptions are elaborated, including kinematics, statics, system construction, actuation, experimental validation, backbone shape identification, motion compensation, manikin trials, etc. The results suggest that it is possible to design a continuum exoskeleton to assist different patients with their limb movements, while no mechanical adjustments on the exoskeleton shall be performed. [DOI: 10.1115/1.4027760]

1 Introduction

Research on exoskeleton attracted a lot of attentions in the past decades. Numerous exoskeleton systems were developed for upper limbs and lower limbs for military or medical applications (e.g., Refs. [1] and [2]). These systems either aim at enhancing a healthy wearer's physical strength with robotic actuation or aim at providing rehabilitation therapies for neuromuscular defects after stroke or injury. Examples include the Mihailo Pupin Institute exoskeleton for paraplegics rehabilitation from the 1970s [3] and many recent advances, such as the performance-enhancing exoskeleton BLEEX [4], the load-carrying leg exoskeleton [5], rehabilitation exoskeletons for lower limbs [6–11], and those for upper limbs [12–19]. Actuation schemes of the aforementioned systems include hydraulic [4] or pneumatic [3,6,17] cylinders, pneumatic muscle actuators [12], cable actuations [9,13,19], parallel mechanisms [10,14,16], gearmotors [20], etc.

Besides these prototypes, research was also about enabling technologies such as inertia compensation [21], sensing and control [5,22–25], novel actuators [26,27], and hyperstaticity avoidance and ergonomics improvements [28–31].

Despite the intended uses for performance enhancement or rehabilitation, many existing exoskeletons followed one similar design concept: using different control and sensing schemes, rigid kinematic chains are actuated to mobilize an attached human wearer. The use of rigid links in an exoskeleton could be justified in applications for strength augmentation to undertake excessive external loads and shield the wearer. But the use of rigid links also introduces drawbacks such as system bulkiness, high inertia, and more importantly the difficulty of maintaining kinematic compatibility between the exoskeleton and the wearer. In strength-augmenting applications where an exoskeleton is usually paired with a specific wearer, the kinematic compatibility could still be properly managed. However, in a rehabilitation clinic where a rigid-link exoskeleton is often shared by a group of patients, it is difficult and inconvenient for a therapist to adjust the exoskeleton from time to time to make sure it fits every patient well.

It might be necessary to specifically design exoskeletons for rehabilitation using compliant elements so that the ideal exoskeleton could automatically conform to different patient anatomies and provide consistent therapies. If more design requirements could be imposed, such an ideal exoskeleton shall be light and comfortable to wear, cheap to manufacture, and compact or even portable for remote or home medicine.

Toward the goals of designing such an ideal exoskeleton for rehabilitation, this paper presents a shoulder exoskeleton incorporating a compliant continuum mechanism as shown in Fig. 1. It will be demonstrated later that this continuum mechanism could passively deform itself to accommodate different patient anatomies while providing pure assistances, when the patient has no or

[1]Corresponding author.

Contributed by the Mechanisms and Robotics Committee of ASME for publication in the Journal of Mechanisms and Robotics. Manuscript received January 14, 2014; final manuscript received May 19, 2014; published online June 19, 2014. Assoc. Editor: Philippe Wenger.

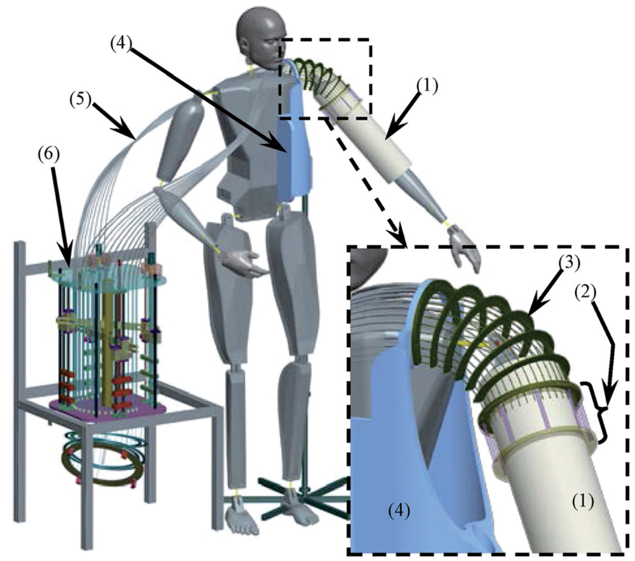

Fig. 1 The continuum shoulder exoskeleton: (1) a rigid armguard, (2) an upper arm sleeve, (3) a flexible continuum shoulder brace, (4) a body vest, (5) a set of guiding cannulae, and (6) an actuation unit

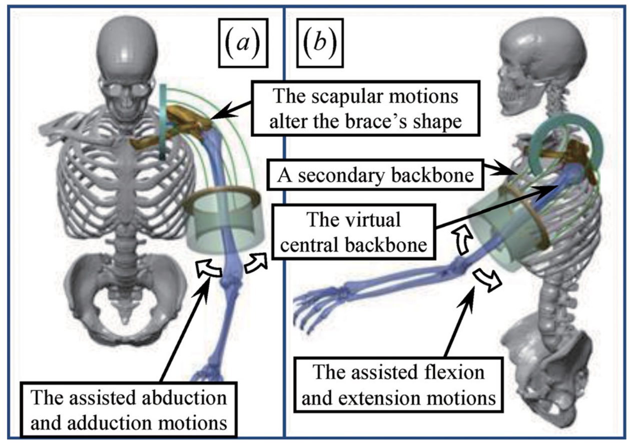

Fig. 2 Design concept of the continuum shoulder exoskeleton: (*a*) the front view and (*b*) the side view

little motor capabilities. The design possesses additional advantages such as light weight, low fabrication cost, and system compactness.

Earlier attempts for designing nonrigid rehabilitation exoskeletons include a simulation work to show the possibility of using elastic cords to assist walking [32], an upper body exoskeleton using home-made pneumatic artificial muscles [33], and a cable-driven upper-limb exoskeleton [18,19].

This paper elaborates the design concept, modeling, system descriptions, shape identification, motion compensation, and manikin trials of the continuum shoulder exoskeleton as shown in Fig. 1. An earlier version of this design with an underperformed hence abandoned actuation unit was presented in Ref. [34]. With a redesigned actuation unit, some preliminary experiments for validating the design concept were presented in Ref. [35]. The shape identification experiments in Ref. [35] was based on imaging processing using a camera. In order to reduce the measurement errors introduced by the lens distortion, all the shape identification experiments in this paper have been redone using an optical tracker. A motion compensation algorithm is added to improve the accuracy of the assisted limb movements. This paper, furthermore, includes an analysis and a series of experiments to quantify the loads on the shoulder joint to indicate the safeness of wearing this exoskeleton on different patients, even with possible scapular motions.

Major contribution of this paper is the design and the experimental characterization of the continuum shoulder exoskeleton. Experimental results show a unique advantage of this design: due to its intrinsic compliance, the continuum exoskeleton passively adapts to different human anatomies and/or mild scapular motions and can always assure the kinematic compatibility between itself and a group of patients while delivering consistent motion assistances. This feature is particularly useful in a clinical setting where a group of patients with no or little motor capabilities share this exoskeleton. Minor contributions of this paper include the design of an actuation unit with a continuum transmission to push and pull flexible members of this exoskeleton in a synchronized manner.

The paper is organized as follows. Section 2 presents the design concept and Sec. 3 presents nomenclature and modeling so that the system descriptions presented in Sec. 4 can be better elaborated. Section 5 presents experimental validation, characterization, motion compensation, and manikin trials of this continuum exoskeleton to show the idea of using one exoskeleton to assist multiple patients without performing any mechanical hardware adjustments. Conclusions and recommended future developments are summarized in Sec. 6.

2 Design Concept

The continuum shoulder exoskeleton as shown in Fig. 1 consists of a rigid armguard, an upper arm sleeve, a flexible continuum brace for the shoulder joint, a body vest, a set of guiding cannulae, and an actuation unit. Actuation of the continuum shoulder brace orients the arm sleeve so as to orient a patient's arm. The armguard is wrapped around the arm to prevent the arm sleeve from rubbing the patient's arm.

Structure of the continuum shoulder brace is also depicted in Figs. 2 and 3. It consists of an end ring, a base ring, a few spacer rings, and several secondary backbones. All the backbones are made from thin NiTi rods (superelastic nickel–titanium alloy).

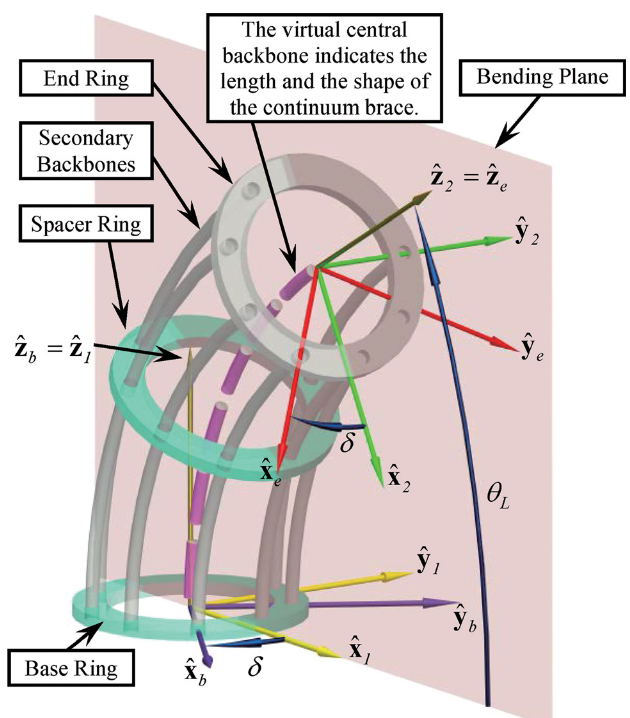

Fig. 3 Nomenclature and coordinates of the continuum brace

The secondary backbones are only attached to the end ring and can slide in holes of the spacer rings and the base ring. Backbones are routed through the set of guiding cannulae to the actuation unit, which simultaneously pulls and pushes these backbones to bend the continuum shoulder brace to orient a patient's arm. Motion capabilities of the continuum brace rely on the back-and-forth bending of the NiTi-made backbones. The fatigue life was shown well above 1×10^5 cycles [36]. Miniature springs are used to keep the spacer rings evenly distributed to prevent buckling of the secondary backbones.

Design of the shoulder brace has considered the mobility of a human shoulder joint as follows:

(i) the arm's abduction/adduction motion in the coronal plane
(ii) the arm's flexion/extension motion in the sagittal plane
(iii) the medial/lateral rotation of the arm (rotation about the axis of the upper arm)
(iv) the scapular retraction/protraction (squeezing/releasing the shoulder blades)
(v) the scapular elevation/depression (the shrugging motion)

A human shoulder joint could hence be approximated as a spherical joint whose center of motion is mobile due to (i) the scapular movements and (ii) the limited contact between the humerus and the scapula.

The flexible continuum shoulder brace is driven by push–pull motions of the backbones, and these push–pull motions are generated from a two-degree of freedom (2-DOF) actuation unit. Referring to Fig. 2, the shoulder brace is actuated to assist the abduction/adduction and the flexion/extension motions of the upper arm.

The upper arm's medial/lateral rotation is not assisted by the current design. A long armguard is hence designed for wrapping the entire arm to prevent the forearm from swinging back and forth. In the current construction, the arm with the armguard can rotate freely inside the arm sleeve.

Particular attentions were directed to the scapular motions. In order to provide as much comfort as possible to a patient, the scapular motions should be allowed, and their movements could lead to constant changes of the pivot point of the arm motions. Referring to Fig. 2, this continuum exoskeleton design would allow such scapular motions, since the continuum shoulder brace would always deform to a new shape which conforms to the scapular motions. The exact actual shape of the continuum brace, which is characterized by a virtual central backbone, depends on a minimum of the potential (gravitational and elastic) energy distributed along the backbones with geometric constraints from the wearer's anatomy.

Imagine the continuum shoulder brace is first actuated to bend and then a patient's limb is inserted. Introduction of the shoulder joint and the weight of the arm would cause the brace to deform further from its settled shape. The additional deflection will allow the brace to accommodate the scapular motions and/or different patient anatomies (e.g., shoulder widths). However, the additional deflection would cause an extra load on the wear's shoulder joint. Section 3.4 presents an elasticity analysis to guide the brace design and Sec. 5.1 presents the experimental results to show that the loads on the shoulder joint could be maintained below a safe threshold for a group of patients with specific joint biomechanics. This exoskeleton would be particularly useful for the rehabilitation of the patients with no or little arm movement capabilities, providing active assistances to the patients while accommodating the patients' different anatomies passively.

Advantages of the continuum exoskeleton include: (i) safety and comfort introduced by the inherent compliance, (ii) passive adaptation to different patient anatomies and scapular motions, (iii) size scalability, (iv) a redundant backbone arrangement for load redistribution and reduced buckling risks, and (v) design compactness achieved by dual roles of these backbones as both the structural components and the motion output members.

3 Nomenclature and Modeling

According to the design concept, the continuum exoskeleton is expected to deform itself to accommodate different patient anatomies or scapular motions while delivering therapeutic motion assistances. A few modeling assumptions would be outlined before the kinematics and statics could be elaborated.

3.1 Modeling Assumptions. Referring to Figs. 2 and 3, shape of the continuum brace is characterized by a virtual central backbone and the modeling assumptions are as follows:

- the brace bends in a planar manner within the bending plane as indicated in Fig. 3
- shapes of the secondary backbones can be characterized by a sweeping motion of the structure's cross section along the virtual central backbone
- the cross section is rigid and is perpendicular to all the backbones
- the secondary backbones are Euler–Bernoulli beams

This work does not assume shape of the brace to be circular, which is different from previously published results [37,38] and will be verified by the experiments.

With severe scapular motions, the assumptions above could fail to hold and particularly the brace's bending shape may not be planar anymore. In such a case, a more general elasticity model might be needed to characterize the kinematics and the statics. In the intended use of this exoskeleton, a patient who could barely move his/her arm might not be strong enough to generate large scapular motions. The experimental characterization presented later also suggests the current modeling could be adequate.

3.2 Nomenclature and Coordinate Systems. The nomenclatures are defined in the nomenclature section and four coordinate systems of the continuum brace are defined as follows:

- *Base Ring Coordinate System* (BRS) is designated as $\{b\} \equiv \{\hat{\mathbf{x}}_b, \hat{\mathbf{y}}_b, \hat{\mathbf{z}}_b\}$. It is attached to the base ring of the continuum brace, whose *XY* plane coincides with the base ring and its origin is at the center of the base. $\hat{\mathbf{x}}_b$ points from the center to the first secondary backbone, whereas $\hat{\mathbf{z}}_b$ is perpendicular to the base ring. The secondary backbones are numbered according to the definition of δ_i.
- *Bending Plane Coordinate System* 1 (BPS1) is designated as $\{1\} \equiv \{\hat{\mathbf{x}}_1, \hat{\mathbf{y}}_1, \hat{\mathbf{z}}_1\}$ which shares its origin with $\{b\}$ and has the continuum brace bending in its *XZ* plane.
- *Bending Plane Coordinate System* 2 (BPS2) is designated as $\{2\} \equiv \{\hat{\mathbf{x}}_2, \hat{\mathbf{y}}_2, \hat{\mathbf{z}}_2\}$ obtained from $\{1\}$ by a rotation about $\hat{\mathbf{y}}_1$ such that $\hat{\mathbf{z}}_1$ becomes backbone tangent at the end ring. Origin of $\{2\}$ is at center of the end ring.
- *End Disk Coordinate System* (EDS) $\{e\} \equiv \{\hat{\mathbf{x}}_e, \hat{\mathbf{y}}_e, \hat{\mathbf{z}}_e\}$ is fixed to the end ring. $\hat{\mathbf{x}}_e$ points from center of the end ring to the first secondary backbone and $\hat{\mathbf{z}}_e$ is normal to the end disk. $\{e\}$ is obtained from $\{2\}$ by a rotation about $\hat{\mathbf{z}}_2$.

3.3 Kinematics. Thorough kinematics analysis of such a continuum brace can be found in Refs. [37–39]. This work emphasizes the shape of the central backbone to be noncircular (the result also applies if the shape is circular). This work also extends the model for an arbitrary arrangement of the secondary backbones by assigning different values to r_i and β_i.

Configuration of the continuum brace is parameterized by $\boldsymbol{\psi} = [\theta_L \quad \delta]^{\mathrm{T}}$. Since shapes of the secondary backbones are assumed by a sweeping motion of the brace's cross section along the central backbone, projection of the *i*th secondary backbone on the bending plane is a curve which is offset by Δ_i from the virtual central backbone. Its radius of curvature and arc-length are indicated by $\rho_i(s_i)$ and s_i. They are related to the parameters of the virtual central backbone as follows:

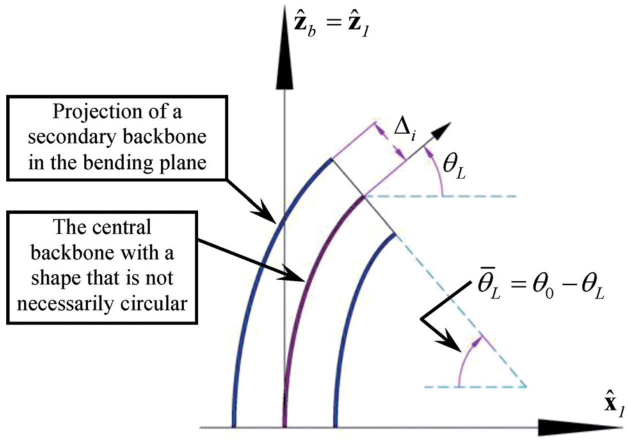

Fig. 4 The central backbone and the projection of secondary backbones in the bending plane

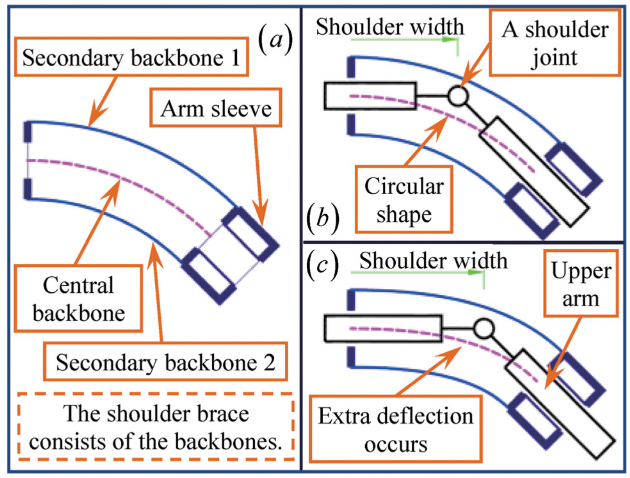

Fig. 5 A simplified 2D case for the elasticity analysis: (*a*) the brace under actuation by itself, and (*b*) and (*c*) the brace worn on a shoulder joint

$$\rho(s) = \rho_i(s_i) + \Delta_i \tag{1}$$

where $\Delta_i \equiv r_i \cos\delta_i$.

The length of the central backbone and the length of the ith backbone are related according to the following integral:

$$L_i = \int ds_i = \int (ds_i - ds + ds) = L + \int (ds_i - ds) \tag{2}$$

Referring to Fig. 4, the integral above can be rewritten as in Eq. (3). Substituting Eq. (1) into Eq. (3) gives Eq. (4), which leads to Eq. (5)

$$\int (ds_i - ds) = \int_0^{\bar{\theta}_L} (\rho_i(s_i) - \rho(s))d\theta \tag{3}$$

$$\int_0^{\bar{\theta}_L} (\rho_i(s_i) - \rho(s))d\theta = -\int_0^{\bar{\theta}_L} \Delta_i d\theta \tag{4}$$

$$L_i = L - r_i \cos\delta_i(\theta_0 - \theta_L) = L + r_i \cos\delta_i(\theta_L - \theta_0) \tag{5}$$

According to the definition of q_i, Eq. (5) gives

$$q_i = r_i \cos\delta_i(\theta_L - \theta_0), \quad i = 1, 2, \ldots, m \tag{6}$$

Equation (6) states that actuation of this continuum brace only depends on the values of θ_L and δ, no matter what the actual shape of the central backbone is. This characteristic provides a particular advantage: when the brace is put on different patients, different anatomies give different shapes of the central backbone, but the actuation remains the same while orienting the limb to the same direction that is characterized by θ_L and δ.

Rotation matrix ${}^{\mathrm{b}}\mathbf{R}_{\mathrm{e}}$ associates $\{e\}$ and $\{b\}$

$${}^{\mathrm{b}}\mathbf{R}_{\mathrm{e}} = R(\hat{\mathbf{z}}_{\mathrm{b}}, -\delta)R(\hat{\mathbf{y}}_1, \theta_0 - \theta_L)R(\hat{\mathbf{z}}_2, \delta) \tag{7}$$

where $R(\hat{\mathbf{n}}, \gamma)$ designates a rotation matrix about $\hat{\mathbf{n}}$ by an angle γ.

The tip position of the continuum brace is given by

$${}^{\mathrm{b}}\mathbf{p}_L = {}^{\mathrm{b}}\mathbf{R}_1 \left[\int_0^L \cos(\theta(s))ds \quad 0 \quad \int_0^L \sin(\theta(s))ds \right]^{\mathrm{T}} \tag{8}$$

where ${}^{\mathrm{b}}\mathbf{R}_1 = R(\hat{\mathbf{z}}_{\mathrm{b}}, -\delta)$ and the integrals above depend on the actual shape of the virtual central backbone.

The tip position ${}^{\mathrm{b}}\mathbf{p}_L$ remains unknown if the exact shape of the brace is not identified. As far as the brace can orient the wearer's upper arm, the exact value of ${}^{\mathrm{b}}\mathbf{p}_L$ is less of concern. In fact, the tip position ${}^{\mathrm{b}}\mathbf{p}_L$ is mobile along the axis of the upper arm due to (i) different bending statuses of the brace, (ii) different anatomical parameters (referring to Fig. 5), and (iii) possible scapular motions.

3.4 An Elasticity Analysis. According to the design concept, once worn on a patient, the continuum exoskeleton is expected to further deflect from its settled shape to accommodate different patient anatomies and/or mild scapular motions. However, the extra deflection would exert additional forces on the shoulder joint. This elasticity analysis could guide the brace design for proper sizes and arrangements of these secondary backbones so that the additional forces would be kept under a safe threshold.

A simplified 2D case is first shown in Fig. 5 to explain the design approach. This explanation could be better understood by only considering the geometry and the brace's elasticity with gravity neglected. The resultant design still possesses the intended features when the gravity is taken into consideration. In the inset (*a*), when the brace is driven according to the actuation kinematics as in Eq. (6), the brace would bend to a circular shape, which has been verified by the analytical and the experimental studies as in Ref. [38]. For this specific bending, it is possible for a patient with a certain shoulder width to wear this brace without causing the brace to deflect more, as shown in the inset (*b*). If the bending is altered or a different shoulder width as in the inset (*c*) is involved, additional deflection of the brace would occur and the shoulder joint would be subject to a load. This load would be different for different shoulder widths and the arm sleeve would translate along the upper arm since the brace's length is constant.

Bending status of the shoulder brace in the inset (*a*) of Fig. 5 corresponds to a minimal elastic potential energy of the brace, since it is not subject to any additional constraints or external disturbances. The brace in the inset (*c*) of Fig. 5 has a higher elastic potential energy due to the presence of the shoulder joint. When the shoulder in the inset (*b*) extends itself to the width as in the inset (*c*), the work done matches the energy increase. If the total elastic potential energy of the brace in the inset (*c*) could be lowered, it would be easier for the brace to adapt to different anatomies or scapular motions.

The total elastic potential energy of the brace is written in Eq. (9). The backbones' bending shapes specified by $\theta(s_i)$ would be determined by (i) a specific bending of the brace (θ_L and δ) and (ii) anatomical geometries and/or scapular motions. The only play to lower the total elastic potential energy is to use less and/or thinner backbones.

$$\Omega = \sum_{i=1}^{m} \int_0^{L_i} \frac{E_i I_i}{2} \left(\frac{d\theta}{ds_i}\right)^2 ds_i \tag{9}$$

According to Ref. [40], an adult's shoulder joint could provide a torque as high as 10 Nm in activities of daily living. Hence, the exoskeleton should be designed strong enough to provide adequate assistance. Actuation of this brace is achieved by pushing and pulling the secondary backbones and using more and thicker backbones will lead to a more rugged design.

When the design's strength requirement conflicts with the compliance requirement, a choice shall be made between (i) less and thicker backbones, or (ii) more and thinner backbones. The latter is preferred since the yielding strength $\propto d_i^2$ while the elastic potential energy Ω (and the gradient $\nabla\Omega$) $\propto I_i \propto d_i^4$. Furthermore, thinner backbones would lead to a smaller bending stress for the same amount of bending. This will hence result in a longer fatigue life, according to the study as in Ref. [36].

Theoretically, an optimization problem can be formulated to generate an optimal arrangement of the secondary backbones. The cost function (to be minimized) could be the maximal force exerted on the shoulder joint, whereas the constraints include (i) the ranges of θ_L and δ values (all the bent configurations of the brace), (ii) the ranges of allowed scapular motions, and (iii) the ranges of targeted patient anatomies (e.g., shoulder widths, etc.).

In fact, it will be difficult to solve such an optimization for these many free variables (L, m, d_i, r_i, β_i, $i = 1, 2, \ldots, m$, $m \geq 3$). This paper hence took an inverse approach by predetermining these design parameters as detailed in Sec. 4.1. Then an experimental study is presented in Sec. 5.1 to quantify the forces exerted on the shoulder joint due to anatomical differences and/or scapular motions. The results could be used to generate an operation manual to indicate the safeness for a patient to use this exoskeleton depending on his/her specific joint biomechanics.

4 System Description

System components of this shoulder exoskeleton mainly include the continuum brace and the actuation unit. Simultaneous actuation of the secondary backbones in the continuum brace orients the wearer's upper arm.

4.1 The Continuum Brace. Main design parameters of the continuum brace include length of brace (L), number, size and placement of the secondary backbones (m, d_i, r_i, and β_i). Length and shape of the brace is characterized by the virtual central backbone.

L and all the r_i are set to 220 mm and 60 mm, respectively, so that the exoskeleton is big enough to fit a reasonable group of patients. The parameters m, d_i, and β_i decide how many backbones, what diameter to use, and where to place them.

Section 3.4 suggests that more and thinner backbones should be used. As shown in Fig. 6, 25 backbones are arranged spanning two-thirds of a circle (the division angle between two adjacent secondary backbones is 10 deg). No backbones were arranged for the armpit area due to the difficulty of routing the backbones to the actuation unit. The backbone arrangement corresponds to the indicated β_i values as shown in Fig. 6. The use of more and thinner backbones brings one additional advantage: failure of one thin backbone would not fail the entire exoskeleton, hence reliability and safety can be potentially increased. The continuum exoskeleton should be capable of providing enough assistance to patients. A simplified statics model which assumes circular shapes of the backbones presented in Ref. [34] estimated that the use of 25 secondary backbones at diameters of 1.2 mm led to a maximal stress in the NiTi material well below the allowed value. Main design parameters are summarized in Table 1.

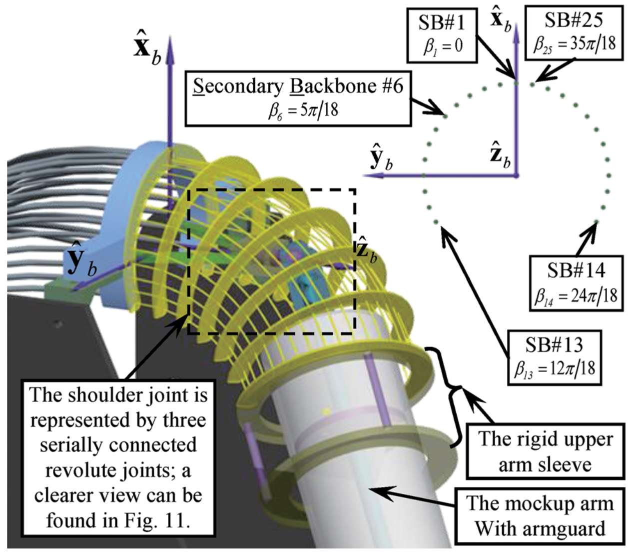

Fig. 6 The continuum brace with the secondary backbone arrangement

4.2 The Actuation Unit and the Transmission. Actuation of the continuum brace involves simultaneous pushing and pulling of 25 secondary backbones. However, as explained in Sec. 3.2, the continuum brace only possesses 2-DOFs to orient a wearer's upper arm. Hence, an important aspect of the actuation unit is to design a transmission system which maps two inputs to 25 outputs according to the actuation kinematics as in Eq. (6).

The attempt of designing such a transmission using hydraulic cylinders was detailed in Ref. [34]. However, that design encountered severe leaking problems and was abandoned. A functional actuation unit is shown in Fig. 7.

The actuation unit has a continuum transmission made from two layers of the continuum structures from Fig. 3:

The inner layer has 25 secondary backbones which are routed to form the shoulder brace through the set of guiding cannulae. Arrangement of these backbones is identical to the brace except that the pitch diameter of this layer is twice of the shoulder brace (all the r_i of the inner layer are twice as big as those of the brace). According to Eq. (6), bending of the inner layer doubles the bending of the shoulder brace.

The outer layer has four secondary backbones that are placed 90 deg away from each other. Bending of this outer layer bends the inner layer to the same orientation, since the end rings of the inner and the outer layers are rigidly attached.

Motorized ball screws push and pull backbones of the outer layer of the continuum transmission. Levers are used to inverse the push–pull motions for backbones with a division angle of 180 deg. A few sliding blocks prevent bulking of these backbones.

This actuation unit design is based on an assumption that the inner layer is bent into a shape similar to that of the outer layer. This assumption was validated by the experiments as in Ref. [35].

5 Experimental Characterization

In order to demonstrate the effectiveness and advantages of the presented continuum shoulder exoskeleton, three sets of experiments were conducted.

Table 1 Design parameters of the continuum brace

$L = 220$ mm	$d_i = 1.2$ mm	$r_i = 60$ mm
$\beta_1 = 0, \beta_2 = \pi/18, \beta_3 = 2\pi/18, \ldots, \beta_{13} = 12\pi/18$		
$\beta_{14} = 24\pi/18, \beta_{15} = 25\pi/18, \ldots, \beta_{25} = 35\pi/18$		

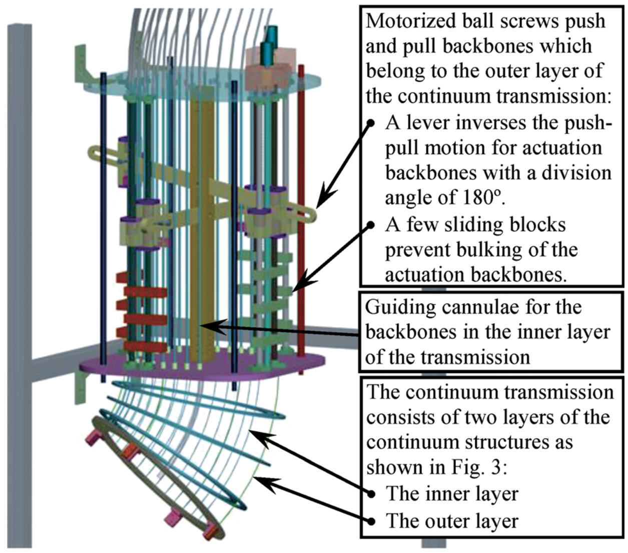

Fig. 7 The actuation unit with a continuum transmission mechanism

5.1 Quantifications of the Forces Exerted on the Shoulder Joint. According to Sec. 3.4, once worn on a shoulder joint, the continuum brace will undergo additional deflections to accommodate anatomical differences and/or scapular motions. The additional deformation would lead to an increase in the force exerted on the shoulder joint. A series of experiments were carried out to quantify the exerted forces. The experimental results could be used to compile an operational manual to indicate the safeness for a patient to use this exoskeleton depending on his/her specific joint biomechanics.

The experimental setup is illustrated in Fig. 8. A white cylinder was used to mimics the arm wrapped in an armguard. Three lead-screw-driven slides are serially connected in a Cartesian form to provide translations in the *XYZ* directions. This could introduce the position change of the center of the shoulder joint, stemmed from anatomical differences and/or scapular motions. Three serially connected revolute joints were used to representing the shoulder joint since an off-the-shelf spherical joint does not have a motion range as big as that of a human shoulder joint. The center of the shoulder joint is considered as the intersecting point P_0 of the axes of the three revolute joints. A 3-axis force sensor (K3D60 from ME-Meßsysteme GmbH with measuring ranges of $\pm 50\,\mathrm{N}$ in *XYZ* directions) was used to measure the loads on the shoulder joint. The sensor was connected to a DAQ card (Advantech PCL-818HG) and a sensing accuracy of 0.08 N in X, Y, or Z directions was achieved.

The shoulder brace was first bent to $\theta_L = 40\,\mathrm{deg}$ and $\delta = 180\,\mathrm{deg}$. In the indicated BRS coordinate system $\{b\} \equiv \{\hat{\mathbf{x}}_b, \hat{\mathbf{y}}_b, \hat{\mathbf{z}}_b\}$ in Fig. 8, the center of the shoulder joint was originally set at a point $P_0 = [0\ 0\ 100\ \mathrm{mm}]^T$. The slides translated the center of the shoulder joint from P_0 to a point $P_1 = [0\ 0\ 130\ \mathrm{mm}]^T$, to another point $P_2 = [0\ 0\ 70\ \mathrm{mm}]^T$ and back to the P_0 point. Then the joint center was translated again from a point $P_3 = [30\ 0\ 100\ \mathrm{mm}]^T$, to a point $P_4 = [30\ 0\ 130\ \mathrm{mm}]^T$, to a point $P_5 = [30\ 0\ 70\ \mathrm{mm}]^T$, and back to the P_3 point. The two translation paths of the center of the shoulder joint are also indicated in the inset of Fig. 8. The path P_5–P_3–P_4 is above the path P_2–P_0–P_1, which could mimic the scapular elevation (the shrugging motion). The readings from the 3D force sensor were converted to $\{b\}$ as plotted in Figs. 9 and 10.

Referring to Figs. 8 and 9, when the center of the shoulder joint is translated from P_0 to P_1, then to P_2 and back to the P_0 point, the force components in the $\hat{\mathbf{x}}_b$ and $\hat{\mathbf{z}}_b$ directions (F_x and F_z) enclose triangular areas in the plot. This is due to the existence of friction between the arm sleeve and the armguard. The averages of F_x and F_z are hence plotted to better reveal the variation trends since the friction in the opposite directions could cancel each other out.

When the center of the shoulder joint is translated between P_2–P_0–P_1, the average of F_x mildly increases, since F_x mainly accounts for the gravity of the mockup arm with armguard. The average of F_z increases from about $-0.8\,\mathrm{N}$ to about 8 N since the translation toward the P_1 point introduces more deformation of the brace. $F_z = 0\,\mathrm{N}$ is a preferable configuration where external forces on the shoulder joint is minimized.

Similar results can be observed in Fig. 10 when the center of the shoulder joint is translated from P_3 to P_4, then to P_5 and back to the P_3 point. The average of F_z is bigger now since the path P_5–P_3–P_4 is radially further away from the central backbone of the brace and hence leads to more deformation of the brace. The average of F_x stays at a similar level since it mainly accounts for the gravity of the arm.

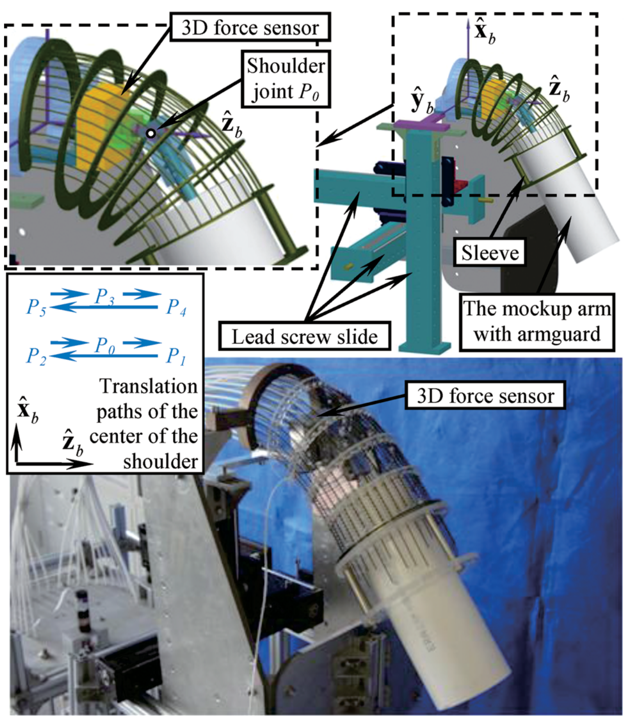

Fig. 8 Experimental setup for the shoulder joint force quantification: (*a*) the CAD model and (*b*) the actual setup

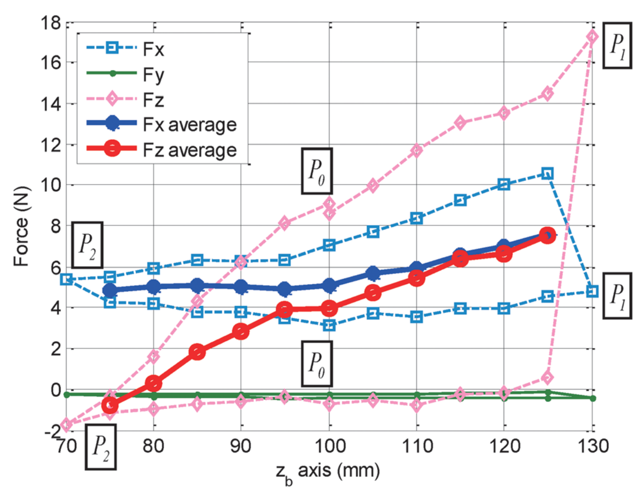

Fig. 9 The shoulder joint forces under movement path P_0–P_1–P_2–P_0

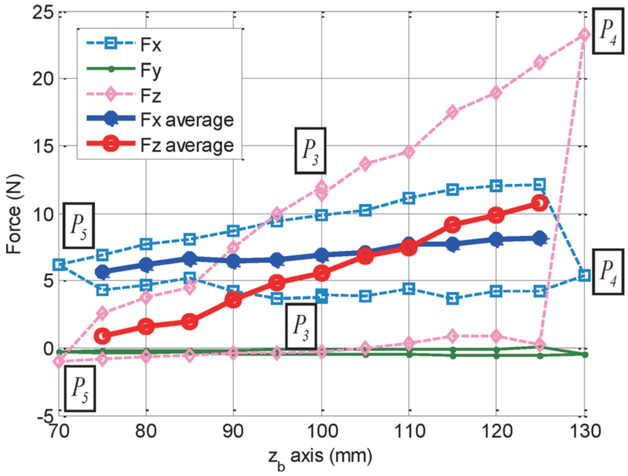

Fig. 10 The shoulder joint forces under movement path P_3–P_4–P_5–P_3

From the results in Figs. 9 and 10, a few insights can be summarized.

- When the shoulder exoskeleton orients an upper arm to an arbitrary direction, different anatomies and/or scapular motions will lead to different loads on the shoulder joint.
- Compliance of the continuum exoskeleton provides an upper bound of the loads on the shoulder joint for a range of anatomical parameters and/or scapular motions. As far as the loads are all under a safety threshold, a patient could use this exoskeleton safely.
- The loads in Fig. 9 are generally smaller than those in Fig. 10, since the path P_2–P_0–P_1 is closer to the center of the brace. Although it could be still safe, wearing the exoskeleton properly or minimizing scapular motions could further reduce the load on the shoulder joint.
- Friction between the armguard and the exoskeleton sleeve may increase the loads on the shoulder joint. It is desirable to reduce this friction in the future developments.

5.2 Shape Identifications and Motion Compensations. The experiments in Sec. 5.1 indicated the safety feature of the exoskeleton, whereas the experiments in this section would demonstrate the effectiveness. It would be shown that the continuum brace deformed differently to passively adapt to different anatomies under the same actuation. Although the deformed shapes of the continuum brace were different, the shoulder exoskeleton managed to orient an upper arm to similar directions.

The shoulder exoskeleton with its actuation unit and the control infrastructure is shown in Fig. 11. Two Maxon DC servomotors (Amax22 110164 with a GP22 gearhead 110340 and a MR encoder 228182) were controlled by a Matlab xPC Target to drive the ball screws with a diameter of 10 mm and a lead of 2 mm according to the kinematics as in Eq. (6). Motion control cards included a D/A card (PCL-727, AdvanTech, Inc.) and a counter card (CNT32-8M, Contec, Inc.).

In the experimental setup in Fig. 11, three serially connected revolute joints approximate the shoulder joint. The center of the shoulder joint is considered as the intersecting point of the axes of the three revolute joints. Different structural components were used to introduce different distances from the shoulder joint center to the base ring of the continuum brace. Different distances could represent different wearer shoulder widths. The distances are 80 mm, 100 mm, and 120 mm, respectively.

Experimental shape identification in Ref. [35] was based on images taken by a camera and imaging processing. In order to reduce the measurement errors due to the lens distortion, all the shape identification experiments were repeated using an optical tracker (Micron Tracker SX60, Claron Technology, Inc.), as

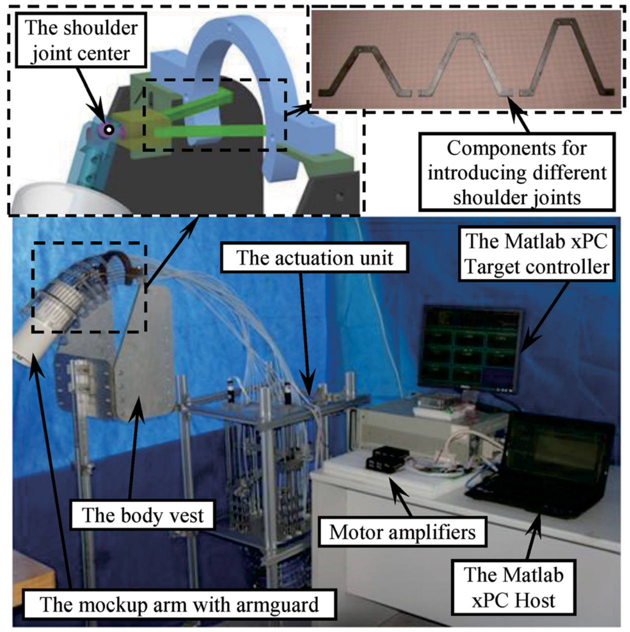

Fig. 11 The shoulder exoskeleton with its actuation unit and controller

shown in the inset (a) of Fig. 12. The tracker recognizes the markers of the pointing tool and directly gives out coordinates of the tool's tip.

Referring to Fig. 12, the exoskeleton was laid down in order to minimize the disturbance from gravity. The arm sleeve slid on a horizontal plate during these shape identification experiments. The plate is made from PTFE to lower the friction. The 100 mm shoulder joint was first used.

The shoulder brace was bent to a configuration of $\theta_L = 50$ deg and $\delta = 180$ deg. Points along the backbone #4, #9, and #12 were sampled using the optical tracker (numbering of the backbones is in Fig. 6). The points were registered to the BRS coordinate system and plotted in Fig. 12. Curves were fitted to these measured points. Using the curve fitting results, a plot of the bending angle versus the curve length can be found in Fig. 13. It is obvious that the shapes of these backbones are not circular anymore (circular shapes will correspond to straight lines in Fig. 13). In Fig. 13, $\theta_L = 50$ deg corresponds to the bending angle $\bar{\theta}_L = 40$ deg. This is why the curves in Fig. 13 end around 38 deg.

The same actuation driving the continuum brace on a 100 mm shoulder joint was repeated for the 80 mm and the 120 mm shoulder joints, and also for the case where no shoulder joint was

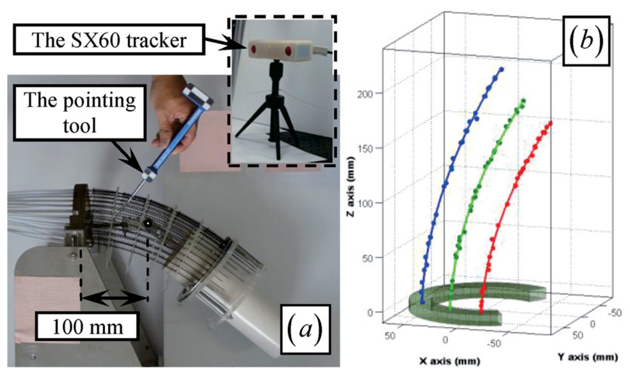

Fig. 12 Shape identification experiments using an optical tracker: (a) the measurement setup and (b) sampled points along three selected backbones (#4, #9, and #12) with the curve fitting results

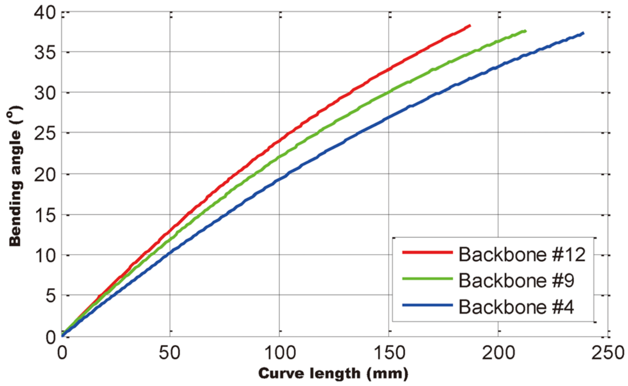

Fig. 13 Bending angles of the selected backbones along their length

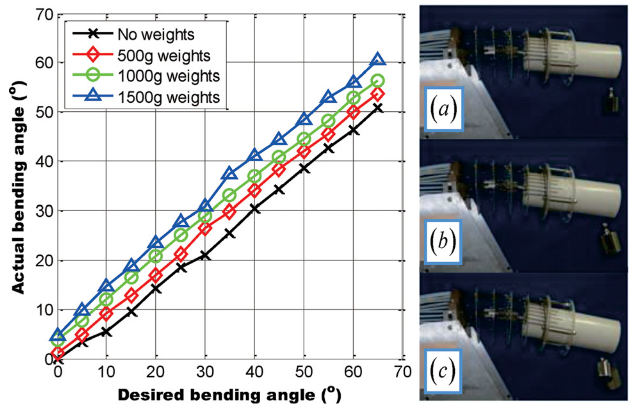

Fig. 15 Actual versus desired bending angles of the continuum brace before motion compensation; the arm with (*a*) a 500 g weight, (*b*) a 1000 g weight, and (*c*) a 1500 g weight

attached. Fig. 14 plots actual bending angles of the continuum brace when the desired bending angels $\bar{\theta}_L$ span from 0 deg to 70 deg. The actual bending is quite close to the desired orientation when the system was laid down and the mockup arm is not subject to gravity.

If the exoskeleton is used in actual rehabilitation therapies, the discrepancy between the desired bending configuration and the actual bending configuration might increase for a heavier arm. As shown in Fig. 15, different weights (500 g, 1000 g, and 1500 g) were attached to the mockup arm. Since the mockup arm is shorter than an entire arm, the weights were hung at the edge to better mimic the center of mass of a straight arm. The actual bending angles were plotted with respect to the desired bending angles $\bar{\theta}_L$. The continuum brace deflected from a horizontal initial configuration when different weights were attached to the mockup arm. This is why the plots in Fig. 15 start at nonzero actual bending angles. The plot of the 1500 g weight is the most above because the attached weight worked with gravity to deflect the brace. Bending discrepancy could be as big as 15 deg before a motion compensation algorithm was implemented.

The motion compensation algorithm presented in Ref. [41] was applied here to reduce the bending discrepancy as in Eq. (10). η is the compensation efficient for the stiffness matrix $\mathbf{K}_d$ of the backbones; the second term $e^{2\mu\phi}\mathbf{K}_\mathbf{c}^{-1}(\eta\boldsymbol{\tau}+\mathbf{f}_\mathbf{s})$ accounts for the stiffness of the backbones in the guiding cannulae where $\boldsymbol{\lambda}$ accounts for system backlashes

$$\boldsymbol{\varepsilon} = \eta\mathbf{K}_\mathbf{d}^{-1}\boldsymbol{\tau} + e^{2\mu\phi}\mathbf{K}_\mathbf{c}^{-1}(\eta\boldsymbol{\tau}+\mathbf{f}_\mathbf{s}) + \boldsymbol{\lambda} \quad (10)$$

where $\boldsymbol{\tau}$ is the tensile loads on the backbones and $\mathbf{f}_\mathbf{s}$ represents a static friction within the guiding cannulae.

For the arm with different weights, different compensation coefficients η ($\eta_{500g} = 1.18$, $\eta_{1000g} = 1.20$, and $\eta_{1500g} = 1.21$) were used so that a bending discrepancy of ± 3 deg was achieved, as shown in Fig. 16.

In a clinical setting, such motion compensation shall be conducted once for every new patient with his/her unique anatomy and arm weight. In the later training sessions, the specific compensation coefficient η would be used for this specific patient. No mechanical adjustments need to be performed on the exoskeleton.

Although the presented motion compensations of the exoskeleton were carried out for the mockup arm with an additional weight up to 1.5 kg, the actual payload capability is beyond this. As mentioned in Sec. 4.1, the continuum brace was designed to be strong enough to provide a 10 Nm torque in the abduction/adduction direction, according to Ref. [34]. Such a torque is big enough to lift a typical human arm whose weight is usually around 4.2 kg (e.g., a 2.3 kg upper arm, a 1.4 kg forearm, and a 0.5 kg hand).

5.3 Manikin Trials. The continuum shoulder exoskeleton was also put on a skeleton manikin to demonstrate the

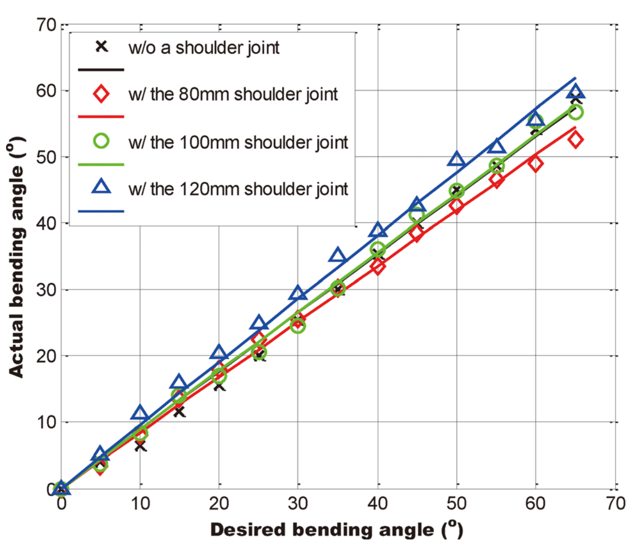

Fig. 14 Actual versus desired bending angles of the continuum brace

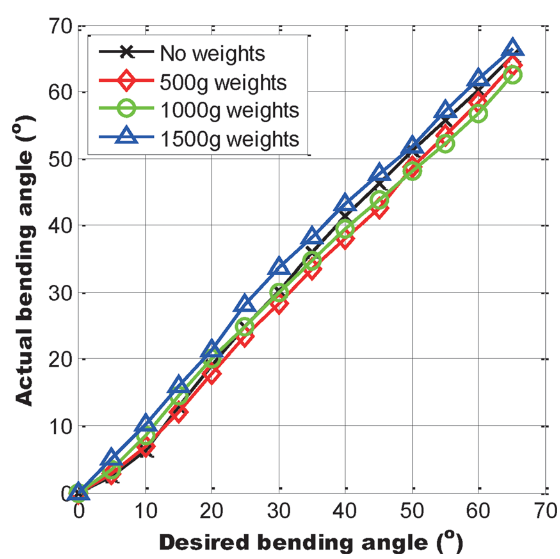

Fig. 16 Actual versus desired bending angles of the continuum brace after the motion compensation

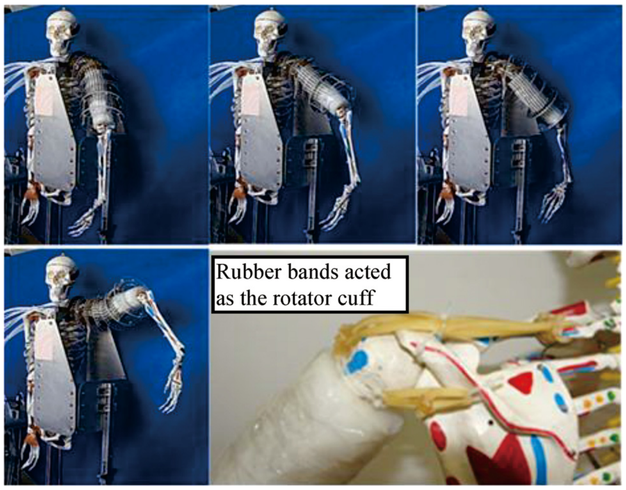

Fig. 17 Manikin trials for the continuum shoulder exoskeleton

effectiveness of the proposed idea. Silicone rubber was molded to the humerus to mimic the upper arm and rubber bands acted as the rotator cuff (including muscles and their tendons) to hold the humerus head in its socket as shown in Fig. 17. Assisted motion of this manikin arm can be also viewed in Fig. 17.

No firm attachment between the arm sleeve and the arm was utilized for the current motion assistance. The armguard was not installed since this is a silicone arm. When the arm sleeve was oriented by the continuum shoulder brace, the silicone arm rested in the sleeve naturally. Even the skeleton with the silicone arm was casually placed inside the exoskeleton, motion assistances were still achieved. The rubber bands were not stretched, which indicated no excessive forces were applied to the shoulder joint.

6 Conclusions and Recommendations

This paper presents the design concept, kinematics, elasticity analysis, component descriptions, and experimental characterizations of a continuum shoulder exoskeleton. The main functional component of the shoulder exoskeleton is a continuum brace. The backbones in the brace were pushed and pulled to orient an arm sleeve and so as to assist a patient with the upper arm motions. While providing assistances, the continuum brace deformed itself and passively adapted to different anatomies and/or possible scapular motions due to its intrinsic flexibility.

The proposed exoskeleton is particularly useful in a clinical environment for the rehabilitation of a group of patients with no or little motor capabilities of their upper limbs (e.g., in an early acute stage of stroke). When the exoskeleton is shared, no hardware adjustments shall be performed to match different patients' anatomies. The exoskeleton can passively deform and adapt to each individual patient's anatomy and/or allow his/her involuntary scapular motions while assisting the upper arm motions. This feature is here referred to as the AAA.

Experimentation was carried out to characterize the features of the shoulder exoskeleton. A 3-axis force sensor was first used to quantify the forces exerted on the shoulder joint with the presence of equivalent scapular motions. The results indicated a safeness threshold for the use of this exoskeleton: if one's shoulder joint strength tolerates the maximal force, the exoskeleton would be safe to use. An optical tracker was then used to identify the backbone shapes with the presence of anatomical differences. Although the shapes of the continuum brace were different for different anatomies, the same actuation was able to assist the anatomically different upper arms with similar motions. Motion compensations were incorporated to reduce the discrepancy between the desired orientation and the actual orientation of the upper arm. When the exoskeleton is shared by a group of patients, each patient with his/her own anatomy and arm weight would possess his/her own compensation coefficients. Without performing any mechanical adjustments, each patient could be assisted using his/her own compensation parameters.

Recommendations for future developments include several aspects. Design ergonomics should be further improved so that it is easy for impaired subjects to wear. A possible solution is to design the shoulder ring as two separable pieces which can be quickly assembled while putting on a patient. What's more, small rolling elements could be added to the arm sleeve to reduce the friction between itself and the armguard. The actuation unit could be further miniaturized to improve the portability of the system. Although the current design is only for the shoulder joint, the ultimate goal is to stack more continuum braces to build a safe, light, multi-DOF exoskeleton to assist the entire arm.

Acknowledgment

The authors would like to thank Professor Nabil Simaan from the Department of Mechanical Engineering, Vanderbilt University, for an early discussion in 2006 which eventually converged to this continuum exoskeleton design.

This work was supported in part by the National Program on Key Basic Research Projects (Grant No. 2011CB013300), in part by Program for New Century Excellent Talents in University (NCET Program), and in part by the by Shanghai Rising-Star Program (Grant No. 14QA1402100).

Nomenclature

d_i = diameter of the ith secondary backbone
E_i = Young's modulus of the ith secondary backbones
i = index of the secondary backbones, $i = 1, 2, \ldots, m$
I_i = cross section moment of inertia of the ith secondary backbone
L, L_i = lengths of the virtual central and the ith secondary backbones measured from the base ring to the end ring
m = number of the secondary backbones
${}^{b}\mathbf{p}(L)$ = tip position and is designated by ${}^{b}\mathbf{p}_L$
${}^{b}\mathbf{p}(s)$ = position vector of a point along the central backbone in the base ring coordinate.
$\mathbf{q}$ = $\mathbf{q} = [q_1 \quad q_2 \quad \cdots \quad q_m]^{\mathrm{T}}$ is the actuation lengths for the secondary backbones and $q_i \equiv L_i - L$
r_i = distance from the virtual central backbone to the ith secondary backbone. r_i can be different for different i
β_i = β_i characterizes the division angle from the ith secondary backbone to the 1st secondary backbone $\beta_1 = 0$ and β_i remain constant once the brace is built
δ = $\delta \equiv \delta_1$ and $\delta_i = \delta + \beta_i$
δ_i = a right-handed rotation angle about $\hat{\mathbf{z}}_1$ from $\hat{\mathbf{x}}_1$ to a ray passing through the central backbone and the ith secondary backbone
$\theta(s)$ = the angle of the tangent to the virtual central backbone in the bending plane. $\theta(L)$ and $\theta(0)$ are designated by θ_L and θ_0, respectively. $\theta_0 = \pi/2$ is a constant
$\bar{\theta}_L$ = due to the definition of $\theta(s)$, a zero bending (a straight configuration) corresponds to $\theta_L = \pi/2$, whereas a 90 deg bending corresponds to $\theta_L = 0$. $\bar{\theta}_L \equiv \pi/2 - \theta_L = \theta_0 - \theta_L$ intuitively indicates how much the continuum brace bends: $\bar{\theta}_L = 0$ for a zero bending and $\bar{\theta}_L = \pi/2$ for a 90 deg bending
$\rho(s)$, $\rho_i(s_i)$ = radius of curvature of the virtual central backbone and the ith secondary backbones, with respect to their lengths s and s_i
$\boldsymbol{\psi}$ = $\boldsymbol{\psi} \equiv [\theta_L \quad \delta]^{\mathrm{T}}$ defines the configuration of the brace
Ω = elastic potential energy of the continuum structure

References

[1] Brewer, B. R., McDowell, S. K., and Worthen-Chaudhari, L. C., 2007, "Poststroke Upper Extremity Rehabilitation: A Review of Robotic Systems and Clinical Results," Top. Stroke Rehabil., **14**(6), pp. 22–44.

[2] Dollar, A. M., and Herr, H., 2008, "Lower Extremity Exoskeletons and Active Orthoses: Challenges and State-of-the-Art," IEEE Trans. Rob., **24**(1), pp. 144–158.

[3] Vukobratovic, M., Hristic, D., and Stojiljkovic, Z., 1974, "Development of Active Anthropomorphic Exoskeletons," Med. Biol. Eng. Comput., **12**(1), pp. 66–80.

[4] Zoss, A. B., Kazerooni, H., and Chu, A., 2006, "Biomechanical Design of the Berkeley Extremity Exoskeleton (BLEEX)," IEEE/ASME Trans. Mechatron., **11**(2), pp. 128–138.

[5] Walsh, C. J., Paluska, D., Pasch, K., Grand, W., Valiente, A., and Herr, H., 2006, "Development of a Lightweight, Underactuated Exoskeleton for Load-Carrying Augmentation," IEEE International Conference on Robotics and Automation (ICRA 2006), Orlando, FL, May 15–19, pp. 3485–3491.

[6] Durfee, W. K., and Rivard, A., 2004, "Preliminary Design and Simulation of a Pneumatic, Stored-Energy, Hybrid Orthosis for Gait Restoration," ASME Paper No. IMECE2004-60075.

[7] Hornby, T. G., Zemon, D. H., and Campbell, D., 2005, "Robotic-Assisted, Body-Weight-Supported Treadmill Training in Individuals Following Motor Incomplete Spinal Cord Injury," Phys. Therapy, **85**(1), pp. 52–66.

[8] Banala, S. K., Agrawal, S. K., Fattah, A., Krishnamoorthy, V., Hsu, W.-L., Scholz, J., and Rudolph, K., 2006, "Gravity-Balancing Leg Orthosis and Its Performance Evaluation," IEEE Trans. Rob., **22**(6), pp. 1228–1239.

[9] Veneman, J. F., Ekkelenkamp, R., Kruidhof, R., van der Helm, F. C. T., and van der Kooij, H., 2006, "A Series Elastic- and Bowden-Cable-Based Actuation System for Use as Torque Actuator in Exoskeleton-Type Robots," Int. J. Rob. Res., **25**(3), pp. 261–281.

[10] Saglia, J. A., Tsagarakis, N. G., Dai, J. S., and Caldwell, D. G., 2009, "A High Performance 2-DOF Over-Actuated Parallel Mechanism for Ankle Rehabilitation," IEEE International Conference on Robotics and Automation (ICRA '09), Kobe, Japan, May 12–17, pp. 2180–2186.

[11] Farris, R. J., Quintero, H. A., and Goldfarb, M., 2011, "Preliminary Evaluation of a Powered Lower Limb Orthosis to Aid Walking in Paraplegic Individuals," IEEE Trans. Neural Syst. Rehabil. Eng., **19**(6), pp. 652–659.

[12] Tsagarakis, N. G., and Caldwell, D. G., 2003, "Development and Control of a 'Soft-Actuated' Exoskeleton for Use in Physiotherapy and Training," Auton. Rob., **15**(1), pp. 21–33.

[13] Perry, J. C., Rosen, J., and Burns, S., 2007, "Upper-Limb Powered Exoskeleton Design," IEEE/ASME Trans. Mechatron., **12**(4), pp. 408–417.

[14] Gupta, A., O'Malley, M. K., Patoglu, V., and Burgar, C., 2008, "Design, Control and Performance of RiceWrist: A Force Feedback Wrist Exoskeleton for Rehabilitation and Training," Int. J. Rob. Res., **27**(2), pp. 233–251.

[15] Stienen, A. H. A., Hekman, E. E. G., Prange, G. B., Jannink, M. J. A., Aalsma, A. M. M., van der Helm, F. C. T., and van der Kooij, H., 2009, "Dampace: Design of an Exoskeleton for Force-Coordination Training in Upper-Extremity Rehabilitation," ASME J. Med. Devices, **3**(3), p. 031003.

[16] Klein, J., Spencer, S., Allington, J., Bobrow, J. E., and Reinkensmeyer, D. J., 2010, "Optimization of a Parallel Shoulder Mechanism to Achieve a High-Force, Low-Mass, Robotic-Arm Exoskeleton," IEEE Trans. Rob., **26**(4), pp. 710–715.

[17] Wolbrecht, E. T., Reinkensmeyer, D. J., and Bobrow, J. E., 2010, "Pneumatic Control of Robots for Rehabilitation," Int. J. Rob. Res., **29**(1), pp. 23–38.

[18] Agrawal, S. K., Dubey, V. N., Gangloff, J. J., Brackbill, E., Mao, Y., and Sangwan, V., 2009, "Design and Optimization of a Cable Driven Upper Arm Exoskeleton," ASME J. Med. Devices, **3**(3), p. 031004.

[19] Mao, Y., and Agrawal, S. K., 2012, "Design of a Cable-Driven Arm Exoskeleton (CAREX) for Neural Rehabilitation," IEEE Trans. Rob., **28**(4), pp. 922–931.

[20] Loureiro, R. C. V., and Harwin, W. S., 2007, "Reach & Grasp Therapy: Design and Control of a 9-DOF Robotic Neuro-Rehabilitation System," IEEE 10th International Conference on Rehabilitation Robotics (ICORR 2007), Noordwijk, Netherlands, June 13–15, pp. 757–763.

[21] Aguirre-Ollinger, G., Colgate, J. E., Peshkin, M. A., and Goswami, A., 2010, "Design of an Active One-Degree-of-Freedom Lower-Limb Exoskeleton With Inertia Compensation," Int. J. Rob. Res., **30**(4), pp. 486–499.

[22] Kawamoto, H., Lee, S., Kanbe, S., and Sankai, Y., 2003, "Power Assist Method for HAL-3 Using EMG-Based Feedback Controller," IEEE International Conference on Systems, Man and Cybernetics, Washington, DC, October 5–8, pp. 1648–1653.

[23] Yamamoto, K., Ishii, M., Noborisaka, H., and Hyodo, K., 2004, "Stand Alone Wearable Power Assisting Suit: Sensing and Control Systems," 13th IEEE International Workshop on Robot and Human Interactive Communication (ROMAN 2004), Kurashiki, Japan, September 20–22, pp. 661–666.

[24] Fleischer, C., and Hommel, G., 2008, "A Human–Exoskeleton Interface Utilizing Electromyography," IEEE Trans. Rob., **24**(4), pp. 872–882.

[25] Sharma, V., McCreery, D. B., Han, M., and Pikov, V., 2010, "Bidirectional Telemetry Controller for Neuroprosthetic Devices," IEEE Trans. Neural Syste. Rehabil. Eng., **18**(1), pp. 67–74.

[26] Stienen, A. H. A., Hekman, E. E. G., ter Braak, H., Aalsma, A. M. M., van der Helm, F. C. T., and van der Kooij, H., 2010, "Design of a Rotational Hydroelastic Actuator for a Powered Exoskeleton for Upper Limb Rehabilitation," IEEE Trans. Biomed. Eng., **57**(3), pp. 728–735.

[27] Bergamasco, M., Salsedo, F., Marcheschi, S., Lucchesi, N., and Fontana, M., 2010, "A Novel Compact and Lightweight Actuator for Wearable Robots," IEEE International Conference on Robotics and Automation (ICRA), Anchorage, AK, May 3–7, pp. 4197–4203.

[28] Schiele, A., and van der Helm, F. C. T., 2006, "Kinematic Design to Improve Ergonomics in Human Machine Interaction," IEEE Trans. Neural Syst. Rehabil. Eng., **14**(4), pp. 456–469.

[29] Kim, H., Miller, L. M., Byl, N., Abrams, G. M., and Rosen, J., 2012, "Redundancy Resolution of the Human Arm and an Upper Limb Exoskeleton," IEEE Trans. Biomed. Eng., **59**(6), pp. 1770–1779.

[30] Sergi, F., Accoto, D., Tagliamonte, N. L., Carpino, G., and Guglielmelli, E., 2011, "A Systematic Graph-Based Method for the Kinematic Synthesis of Non-Anthropomorphic Wearable Robots for the Lower Limbs," Front. Mech. Eng., **6**(1), pp. 61–70.

[31] Jarrassé, N., and Morel, G., 2012, "Connecting a Human Limb to an Exoskeleton," IEEE Trans. Rob., **28**(3), pp. 697–709.

[32] van den Bogert, A. J., 2003, "Exotendons for Assistance of Human Locomotion," Biomed. Eng. Online, **2**(17), pp. 1–8.

[33] Kobayashi, H., and Hiramatsu, K., 2004, "Development of Muscle Suit for Upper Limb," IEEE International Conference on Robotics and Automation (ICRA '04), New Orleans, LA, April 26–May 1, pp. 2480–2485.

[34] Xu, K., Qiu, D., and Simaan, N., 2011, "A Pilot Investigation of Continuum Robots as a Design Alternative for Upper Extremity Exoskeletons," IEEE International Conference on Robotics and Biomimetics (ROBIO), Phuket, Thailand, December 7–11, pp. 656–662.

[35] Xu, K., and Qiu, D., 2013, "Experimental Design Verification of a Compliant Shoulder Exoskeleton," IEEE International Conference on Robotics and Automation (ICRA), Karlsruhe, Germany, May 6–10, pp. 3894–3901.

[36] Matsui, R., Tobushi, H., Furuichi, Y., and Horikawa, H., 2004, "Tensile Deformation and Rotating-Bending Fatigue Properties of a Highelastic Thin Wire, a Superelastic Thin Wire, and a Superelastic Thin Tube of NiTi Alloys," ASME J. Eng. Mater. Technol., **126**(4), pp. 384–391.

[37] Xu, K., and Simaan, N., 2008, "An Investigation of the Intrinsic Force Sensing Capabilities of Continuum Robots," IEEE Trans. Rob., **24**(3), pp. 576–587.

[38] Xu, K., and Simaan, N., 2010, "Analytic Formulation for the Kinematics, Statics and Shape Restoration of Multibackbone Continuum Robots Via Elliptic Integrals,"ASME J. Mech. Rob., **2**(1), p. 011006.

[39] Webster, R. J., and Jones, B. A., 2010, "Design and Kinematic Modeling of Constant Curvature Continuum Robots: A Review," Int. J. Rob. Res., **29**(13), pp. 1661–1683.

[40] Rosen, J., Perry, J. C., Manning, N., Burns, S., and Hannaford, B., 2005, "The Human Arm Kinematics and Dynamics During Daily Activities—Toward a 7 DOF Upper Limb Powered Exoskeleton," 12th International Conference on Advanced Robotics (ICAR '05), Seattle, WA, July 18–20, pp. 532–539.

[41] Simaan, N., Xu, K., Kapoor, A., Wei, W., Kazanzides, P., Flint, P., and Taylor, R. H., 2009, "Design and Integration of a Telerobotic System for Minimally Invasive Surgery of the Throat," Int. J. Rob. Res., **28**(9), pp. 1134–1153.